

A Physical Metric for Inertial Confinement Fusion Capsules

Baolian Cheng *  and Paul A. Bradley

Los Alamos National Laboratory, Los Alamos, NM 87545, USA; pbradley@lanl.gov

* Correspondence: bcheng@lanl.gov

Abstract: The performance of fusion capsules on the National Ignition Facility (NIF) is strongly affected by the physical properties of the hot deuterium–tritium (DT) fuel, such as the mass, areal density, and pressure of the hot spot at the stagnation time. All of these critical quantities depend on one measured quantity, which is the ratio of the specific peak implosion energy to the specific internal energy of the hot spot. This unique physical quantity not only can measure the incremental progress of the inertial confinement fusion capsules towards ignition but also measures the conversion of the peak implosion kinetic energy of the pusher shell into the internal energy of the hot fuel in a capsule. Analysis of existing NIF shots to date are performed. The ratio metric is compared quantitatively with the ignition criterion. Results provide new perspectives on the NIF experiments by which the performance of the burning plasma can be determined and controlled through the fine tune of the implosion parameters, which improves future designs and predictions of the ignition capsules.

Keywords: inertial confinement fusion; thermonuclear ignition

1. Introduction

Recently, fusion capsule performance has been improved enormously on the National Ignition Facility (NIF) by using two designs: a shaped non-cylindrical hohlraum to delay plasma filling for better inner-beam propagation (I-Raum) and high-yield big-radius implosion design (Hybrid) [1–7] together with finely manufactured capsules with much smoother capsule surfaces and smaller-diameter fill tubes [1,5]. The Hybrid-E design also increased the amount of energy delivered to the hot spot by increasing the capsule radius by 15% compared to previous experiments [8–22] and reduced the hohlraum scale at a fixed capsule size compared to previous Hybrid designs, thereby increasing the hohlraum efficiency and energy coupled to the capsule. The highest neutron yield of 1.35 MJ then was achieved in shot N210808 [1,6] through several design optimizations. In order to systematically characterize the design progress and continuous improvements of the capsules towards a robust burning plasma and ignition, it is useful to introduce an observable metric to measure the incremental design progress of the capsules relative to the ignition criteria.

The paper is organized as follows. Theory and detailed analysis of the new metric are given in Section 2. Section 3 presents expanded discussions on key physics concepts, including important time scales in inertial confinement fusion and a comparison of existing ignition metrics. Conclusion are given in Section 4.

2. Theory and Analysis

In the framework of the minimal energy implosion model [23–25], the physical properties of the hot fuel in an inertial confinement fusion (ICF) capsule are described by the peak implosion kinetic energy. Given an implosion energy, there is an optimal (or maximum) hot-spot pressure (P_{hs}), which can be expressed in terms of the peak implosion velocity (V_{imp}) and the pusher adiabat [23], and has the expression

$$P_{hs} = P_0 \left[\frac{\gamma_p}{(3\gamma_p - 1)\epsilon_0} \eta V_{imp}^2 \right]^{\frac{\gamma_p}{\gamma_p - 1}}. \quad (1)$$



Citation: Cheng, B.; Bradley, P.A. A Physical Metric for Inertial Confinement Fusion Capsules. *Plasma* **2024**, *7*, 146–159. <https://doi.org/10.3390/plasma7010010>

Academic Editor: Andrey Starikovskiy

Received: 14 January 2024

Revised: 14 February 2024

Accepted: 16 February 2024

Published: 21 February 2024



Copyright: © 2024 by the authors. Licensee MDPI, Basel, Switzerland. This article is an open access article distributed under the terms and conditions of the Creative Commons Attribution (CC BY) license (<https://creativecommons.org/licenses/by/4.0/>).

Here, the pusher is the sum of the remaining ablator and cold fuel for the NIF point design. The pusher adiabat is closely related to the effective adiabatic index of the pusher (γ_p) [26,27]. For a high-adiabat pusher—effective adiabat index $\gamma_p \approx 5/3$ —Equation (1) gives $P_{hs} \propto V_{imp}^5$ [23,28], which is in good agreement with the NIF experimental data [29,30] and differs from the scaling law $P_{hs} \propto V_{imp}^3$ predicted by many simulations and theoretical models [6,31,32]. Although most NIF experiments do not have an optimal energy partition between hot spot and pusher and the implosion energy has not yet been minimized, optimizing the thickness of the pusher is a necessary step to achieve optimal energy split and MJ performance using a minimal implosion energy.

In Equation (1), P_0 , ρ_0 , and ϵ_0 are, respectively, the pressure, mass density, and specific internal energy of the pusher at the time of the peak implosion velocity. η is a coefficient accounting for the fraction of the total peak implosion energy going into the compression of the capsule (radially). Assuming a gamma law equation of state (EOS) for the cold deuterium–tritium fuel, $P/P_0 = (\rho/\rho_0)^{\gamma_p}$ and $\epsilon_p = \epsilon_0(P/P_0)^{\frac{\gamma_p-1}{\gamma_p}}$, then the ratio of the hot-spot mass (M_{hs}) to the pusher mass (M_p) has the expression

$$\frac{M_{hs}}{M_p} = \frac{(\gamma_p - 1)\eta V_{imp}^2}{(3\gamma_p - 1)2\epsilon_{hs}}, \tag{2}$$

where $\epsilon_{hs} = 2RT/[A_{DT}(\gamma_g - 1)]$ represents the specific internal energy of the hot DT prior to self-heating by alpha particle deposition, T is the peak no-burn temperature of the hot spot, A_{DT} is the average atomic mass of the DT mixture, R is the gas constant and γ_g is the adiabatic index of the DT.

We would like to point out that, although the energy losses from radiation and thermal conduction during the implosion phase (i.e., the phase of assembling the hot spot prior to alpha-heating) are not explicitly itemized in the minimal energy model, the coefficient $(1 - \eta)$ actually accounts for all other energies and energy losses that do not involve the compression of the hot-spot and pusher [23]. Simulations show that the energy losses from radiation and thermal conduction during implosion are negligible compared to the internal energy of the hot spot at maximum compression (see Figure 2 in reference [6]). All energy losses during the phase of TN burn and fusion expansion of the hot spot are taken into account by the requirement of energy doubling of the hot-spot during the hydrodynamic disassembly time in the ignition theory developed by Cheng et al. [23–25,33]. More discussions are given in Section 3.

2.1. Metric \tilde{v}

Now, we define an observable metric \tilde{v} as the ratio of the specific peak kinetic energy ($\eta V_{imp}^2/2$) to the specific internal energy of the hot spot (ϵ_{hs}):

$$\tilde{v} \equiv \eta \frac{V_{imp}^2}{2} / \epsilon_{hs} = \frac{5}{12} \eta \frac{V_{imp}^2}{RT}, \tag{3}$$

where $A_{DT} = 2.5$ and $\gamma_g = 5/3$ have been applied. In Expression (3), the peak implosion velocity can be measured through ConA experiments by maintaining the same design configuration and implosion conditions and can also be inferred from simulations that match the ConA and VISAR data. The DT temperature is usually obtained from the variance of the Doppler-broadened 14 MeV DT neutron spectra. At the NIF, the DT temperature is measured using several neutron-time-of-flight (NTOF) detectors arrayed around the target chamber. However, the 14 MeV neutron peak can be broadened not only by thermal ion motion but also by the presence of residual velocity flow, or residual kinetic energy (RKE), in the hot spot resulting from incomplete conversion of implosion kinetic to thermal energy at peak compression. In this case, the variance of the 14 MeV neutron peak corresponds to an apparent temperature, T_{app} , which is the sum of the neutron-weighted thermal ion temperature and the neutron-weighted bulk fluid velocity variance along the detector line-

of-sight [15,34,35] The efficiency η is usually not measured, but it can be estimated using expression $\eta \simeq 1 - (1 + M_{hs}/M_p)(V_{RKE}/V_{imp})^2$, where we have neglected any rotation and vibration of the capsule as well as the energy losses during implosion (as discussed earlier) and V_{RKE} represents the residual velocity of the flow in the hot spot and pusher at peak compression. For $M_{hs}/M_p \sim 1/10$ and $V_{RKE}/V_{imp} < 1/5$ (e.g., $V_{RKE} \sim 68$ km/s and $V_{imp} \sim 391$ km/s in N210808 [1,2,6]), $\eta \simeq 0.96$. For convenience, we take $\eta \sim 0.96$ for most NIF experiments.

In terms of \tilde{v} , the mass ratio (2) and other hot-spot physical parameters, such as the ratios of energy, mass density, and areal density of the hot spot to pusher, are given as follows [23]:

$$\frac{M_{hs}}{M_p} = \frac{(\gamma_p - 1)}{(3\gamma_p - 1)} \tilde{v}, \tag{4}$$

$$\frac{E_{hs}}{E_p} = \frac{\gamma_p - 1}{2\gamma_p}, \quad \frac{E_{hs}}{E_{tot}} = \frac{\gamma_p - 1}{3\gamma_p - 1}, \quad \frac{V_{hs}}{V_p} = \frac{1}{3\gamma_p}, \tag{5}$$

$$\frac{\rho_{hs}}{\rho_p} = 3\gamma_p \frac{(\gamma_p - 1)}{(3\gamma_p - 1)} \tilde{v}, \tag{6}$$

$$\frac{(\rho R)_{hs}}{(\rho R)_p} = \psi(\gamma_p) \tilde{v}, \quad \frac{(\rho R)_{hs}}{(\rho R)_{tot}} = \frac{\psi(\gamma_p) \tilde{v}}{1 + \psi(\gamma_p) \tilde{v}}, \tag{7}$$

where $\psi(\gamma_p) \equiv [(1 + 3\gamma_p)^{1/3} + (1 + 3\gamma_p)^{2/3} + 1](\gamma_p - 1)/(3\gamma_p - 1)$ is a function of the adiabatic index of the hot spot and the pusher [23]. E_p , V_p , ρ_p , and $(\rho R)_p$ are the energy, volume, mass density, and areal density of the pusher, respectively. Similarly, E_{hs} , V_{hs} , ρ_{hs} , and $(\rho R)_{hs}$ are the corresponding physical quantities of the hot spot. $(\rho R)_{tot}$ is the total areal density of the capsule that includes hot spot and pusher (the sum of cold fuel and remaining ablator), i.e., $(\rho R)_{tot} \equiv (\rho R)_{hs} + (\rho R)_p$ and $(\rho R)_p \equiv \rho_{cf}(R_{cf} - R_{hs}) + \rho_{ra}\Delta R_{ra}$, where ρ_{cf} and R_{cf} are, respectively, the mass density and outer radius of the cold DT fuel, ρ_{ra} is the mass density of the remaining ablator, and $\Delta R_{ra} \equiv R_p - R_{cf}$ is the thickness of the remaining ablator.

At the time of peak implosion velocity, nearly all of the energy into the capsule in the radial direction is in the form of kinetic energy of the pusher. At stagnation time, nearly all of the kinetic energy is converted into the internal energy of the system, i.e., the sum of the internal energy of the pusher and the hot spot. We assume 4% of the total peak implosion energy becoming residual kinetic energy in the capsule in this analysis. The higher the hot spot internal energy, the better the energy conversion of the capsule and the more robustly the hot spot burns. Therefore, the ratio of the specific peak kinetic energy to the specific internal energy of the hot spot, \tilde{v} , given by Equation (3), is an important measure to quantify the energy conversion of the capsule during implosion. Substituting the gas constant R into \tilde{v} reduces Equation (3) to

$$\tilde{v} = 4.32\eta \frac{V_{imp}^2}{T(\text{keV})}, \tag{8}$$

where the peak implosion velocity (V_{imp}) is in units of 1000 km per second and the peak no-burn temperature of the hot spot, T , is in keV.

If there is no alpha heating, the peak no-burn temperature (T_{pnb}) is the measured hot-spot temperature, as in the early NIF shots during the National Ignition Campaign (NIC). In the presence of alpha heating, the measured temperature (T_{hs}) is the sum of the peak no-burn temperature and the temperature increase (ΔT) due to alpha heating, that is, $T_{hs} = T_{pnb} + \Delta T$. Thus, in terms of T_{hs} , the expression \tilde{v} can be written as

$$\tilde{v} = 4.32\eta \frac{V_{imp}^2}{T_{hs} - \Delta T} \simeq 4.32\eta \frac{V_{imp}^2/T_{hs}}{1 - \Delta T/T_{hs}} \geq v_o. \tag{9}$$

where $\tilde{v}_o \equiv 4.32\eta V_{imp}^2/T_{hs}$ is defined as the observed specific energy ratio of the hot spot. In the absence of alpha heating, $\Delta T \simeq 0$ and $\tilde{v} = \tilde{v}_o$.

Equation (9) shows that, for a given peak implosion velocity, the measured \tilde{v}_o of the hot spot is always less than the peak no-burn \tilde{v} if alpha-heating is present in the capsule. The dependence of the ratio of the hot-spot areal density $(\rho R)_{hs}$ to the total areal density $(\rho R)_{tot}$ on \tilde{v} is demonstrated in Figure 1, from which we see that the hot-spot areal density increases with the specific energy ratio \tilde{v} .

In terms of metric \tilde{v} , the original NIF ignition criteria $(\rho R)_{hs} \geq 0.3 \text{ g/cm}^2$ and $(\rho R)_{tot} = 1 \text{ g/cm}^2$ at $T \simeq 4.5 \text{ keV}$ [31] would become condition $\tilde{v} \geq 0.43/\psi(\gamma_p)$. For a low-adiabat ($\alpha \sim 1.5$) pusher, $\psi(\gamma_p) \simeq 1.95$ and $\tilde{v} \geq 0.22$; for a high-adiabat ($\alpha \sim 3$) pusher, $\psi(\gamma_p) \simeq 1.02$ and $\tilde{v} \geq 0.42$ will be required. A detailed description of the physical variables is displayed in Table 1, which shows the relationship between the critical variables of the capsule and the specific energy ratio at the various pusher adiabats.

Table 1. The relationship between the hot-spot variables and metric $\nu \equiv 3\tilde{v}$ at various pusher adiabats. $\Delta_p \equiv R_p - R_{hs}$ is the thickness of the pusher at the stagnation time; here, R_p is the outer radius of the pusher.

Adiabat	Theory		
	$\gamma_p = 4/3$	$\gamma_p = 5/3$	$\gamma_p = 3$
Δ_p / R_{hs}	0.71	0.816	1.153
E_{hs} / E_p	1/8	1/5	1/3
E_{hs} / E_{tot}	1/9	1/6	1/4
V_{hs} / V_p	1/4	1/5	1/9
M_{hs} / M_p	$\nu/27$	$\nu/18$	$\nu/12$
$(\rho R)_{hs} / (\rho R)_p$	0.21ν	0.34ν	0.65ν
ρ_{hs} / ρ_p	0.148ν	0.28ν	0.75ν
$(\rho R)_{tot} / (\rho R)_{hs}$	$4.76/\nu + 1$	$2.94/\nu + 1$	$1.54/\nu + 1$

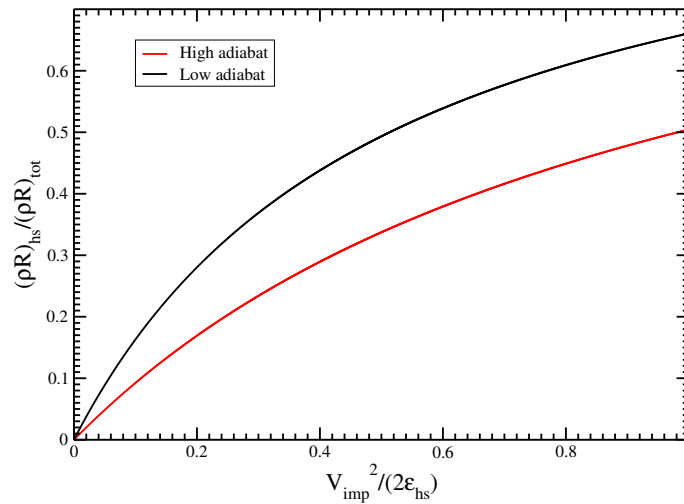


Figure 1. The dependence of the ratios of hot-spot areal density to the total areal density on the specific energy ratio \tilde{v} . The red solid line represents the high pusher adiabat ($\alpha \sim 3$) case and the black solid line expresses the low pusher adiabat ($\alpha \sim 1.5$) case.

The goal of the NIF capsule design is to maximize conversion of the implosion kinetic energy to hot-spot internal energy to produce a self-sustained thermonuclear burn on the hot spot. The specific energy ratio of the hot spot is able to capture the incremental progress of the design of the NIF ignition capsules and also remains sensible and robust at gain $\gg 1$.

2.2. Ignition Criterion in Various Forms

The $\rho R - T$ condition [24,25,33] for the hot spot to have self-sustained TN burn is given by

$$(\rho R)_{hs} \geq \Phi(T), \tag{10}$$

where

$$\Phi(T) \equiv \frac{[(1+d)^2/d](E/n_{DT})C_s^*A_{DT}}{[\langle\sigma v\rangle W_\alpha - \dot{Q}_l(1+d)^2/(dn_{DT}^2)]\tilde{g}N_A},$$

in which E is the total energy of the hot spot [23], i.e., the sum of the energies of ions, electrons, and radiation. Thermal equilibrium between ions and electrons is assumed in the derivation. $n_{DT} \equiv \rho_{DT}N_A/A_{DT}$, ρ_{DT} is the mass density of the hot DT; $d = N_D/N_T$ is the D to T ratio, where N_D and N_T are, respectively, the total numbers of deuterium and tritium atoms in moles; $\langle\sigma v\rangle$ is the DT nuclear reaction rate; and $W_\alpha \equiv 3.52f_\alpha + 14f_n$ MeV is the energy deposited into the hot DT per fusion reaction. f_α is the fraction of the α -particle kinetic energy and f_n is the fraction of the 14 MeV fusion neutron energy deposited in the fuel. In most cases, $f_n \sim 0$ because the mean free path of the 14 MeV neutrons is much larger than the hot-spot radius R_{hs} . f_α is determined using the formula given in Ref. [36]. The effective sound speed C_s^* is equal to the sound speed C_s in the hot spot divided by the tamping factor f_T , but the tamping factor in the NIF point design capsule is almost negligible because f_T is proportional to the value of $\sqrt{\rho_p/\rho_{hs}}$ [26] at the boundary between the hot spot and the cold fuel. In the NIF point design, this boundary is smooth in density due to the nature of continuous plasma of the cold fuel, i.e., $\rho_p \sim \rho_h$ at the boundary and, hence, f_T has a value of ~ 1 [26,33]. N_A is Avogadro's number and \tilde{g} is a shape factor having a value of 1 for spherical and < 1 for non-spherical hot spots [37]. $\dot{Q}_l \equiv dQ_l/dt$ denotes the energy loss rate from bremsstrahlung emission and electron heat conduction. For DT temperatures of $3 \text{ keV} < T < 5 \text{ keV}$, $\Phi(T) \approx 4\kappa_c/(f_T\tilde{g})/T^{2.5} \text{ g/cm}^2$, and, for $5 \text{ keV} \leq T \leq 10 \text{ keV}$, $\Phi(T) \approx 2.063\kappa_c/(f_T\tilde{g})/T^{2.0} \text{ g/cm}^2$, where $\kappa_c \approx 5.514$ [33].

An alternative expression of the ignition condition in (10) is the minimum hot-spot mass [24,25,33]:

$$M_{hs}^{min} \geq I(T) \frac{[R_0(\text{cm})/C_f]^2}{(\tilde{g}f_T)} \text{ g}, \tag{11}$$

where

$$I(T) = \begin{cases} 92.34/T^{2.5}(\text{keV}) & \text{if } 3 < T < 5 \text{ keV}, \\ 47.63/T^{2.0}(\text{keV}) & \text{if } 5 < T < 10 \text{ keV}. \end{cases} \tag{12}$$

$C_f \equiv R_0/R_{hs}$ is the convergence ratio and R_0 is the initial radius of the pusher (\sim the initial radius of the DT fuel). Substituting Equations (4) and (10) into Equation (11) gives the requirement for the specific energy ratio of the hot spot:

$$\tilde{v} \geq \frac{(3\gamma_p - 1)}{(\gamma_p - 1)M_p(\text{g})} \frac{I(T)}{\tilde{g}f_T} \left[\frac{R_0(\text{cm})}{C_f} \right]^2, \tag{13}$$

and, for the total areal density of the capsule,

$$(\rho R)_{tot} \geq \frac{(1 + \psi\tilde{v})}{\psi\tilde{v}} \Phi(T) \tag{14}$$

to have self-sustained TN burn. If the remaining ablator mass is comparable to the mass of the cold fuel, as demonstrated in NIF simulations, assuming spherical symmetry and uniform density distribution, we have $\rho_{ra}(R_p^3 - R_{cf}^3) \simeq \rho_{cf}(R_{cf}^3 - R_{hs}^3)$, which gives a relationship $(\rho R)_{ra} \leq (\rho R)_{cf}(1 + R_{hs}/R_{cf} + R_{hs}^2/R_{cf}^2)/3$; here, an approximation of $R_p \sim R_{cf}$ is used for simplicity. At peak compression, $R_{cf} \simeq (1 + 3\gamma_p)^{1/3}R_{hs}$ [24,26]. Thus, $(\rho R)_{ra} \approx (\rho R)_{cf}[1 + (1 + 3\gamma_p)^{-1/3} + (1 + 3\gamma_p)^{-2/3}]/3 \equiv f_{ra}(\rho R)_{cf}$, and $f_{ra} \equiv (\rho R)_{ra}/(\rho R)_{cf} = [1 + (1 + 3\gamma_p)^{-1/3} + (1 + 3\gamma_p)^{-2/3}]/3$. For high adiabat, $f_{ra} \simeq 0.62$ and, for low adiabat, $f_{ra} \simeq 0.56$. Substituting these into $(\rho R)_{tot}$ gives $(\rho R)_{tot} = (1 + f_{ra})(\rho R)_{fuel} - f_{ra}(\rho R)_{hs}$.

Because the measured areal density of the fuel is proportional to the neutron downscattered ratio (DSR), i.e., $(\rho R)_{fuel} \approx 21DSR$ [31], we can rewrite Condition (14) into the form

$$DSR \geq \frac{[1 + f_{ra} + 1/(\psi\tilde{\nu})]}{21(1 + f_{ra})} \Phi(T). \tag{15}$$

Substituting $\Phi(T)$ into Equation (15) gives

$$DSR \geq \frac{[1 + f_{ra} + 1/(\psi\tilde{\nu})]}{21(1 + f_{ra})} \left(\frac{22.06}{f_T \bar{g}}\right) \left(\frac{T}{\text{keV}}\right)^{-2.5} \tag{16}$$

for $3 \text{ keV} < T < 5 \text{ keV}$ and

$$DSR \geq \frac{[1 + f_{ra} + 1/(\psi\tilde{\nu})]}{21(1 + f_{ra})} \left(\frac{11.38}{f_T \bar{g}}\right) \left(\frac{T}{\text{keV}}\right)^{-2.0} \tag{17}$$

for $5 \text{ keV} < T < 10 \text{ keV}$.

The temperature dependences of $\tilde{\nu}$ and DSR are plotted in Figures 2 and 3, respectively. In the figures, the red solid line represents the theoretical threshold for having a self-sustained TN burn hot spot in a capsule with a high pusher adiabat. The blue dashed line represents the theoretical threshold for an ignition capsule with a low pusher adiabat. The open circles are the NIF data. Here, we would like to point out that the specific energy ratios corresponding to the NIF data are the measured $\tilde{\nu}_o$ values because the observed hot-spot temperature was used in the calculations. The peak no-burn $\tilde{\nu}$ values in these capsules should be higher than the observed $\tilde{\nu}_o$ values. For many NIF shots, $\tilde{\nu} \sim \tilde{\nu}_o$ because the alpha heating was minimal in the capsules. By Criterion (13), N210808 achieved ignition on the hot spot [6] but failed to propagate the TN burn. Propagation burn is important for many applications; the difficulty in achieving successful TN burn propagation in the point design will be presented in a separate paper.

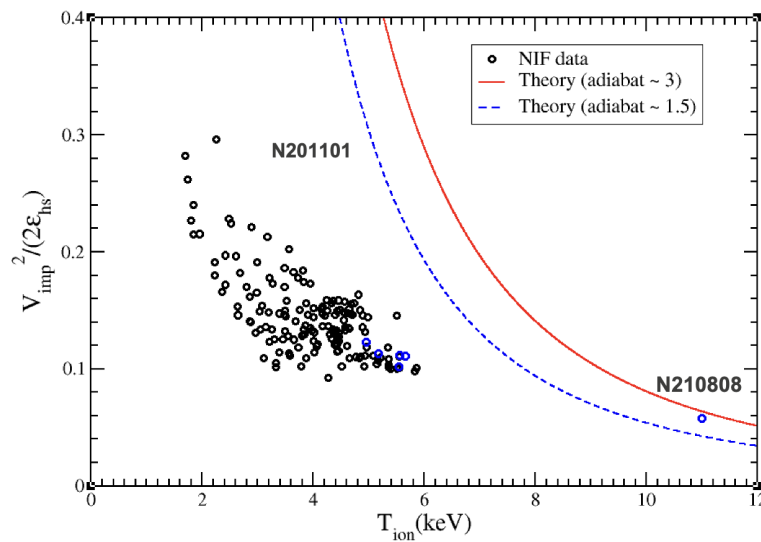


Figure 2. The minimum required specific energy ratio of the hot spot for self-sustained TN burn as a function of the hot-spot temperature. The red solid line is the theoretical threshold for self-sustained burn for capsules with high-adiabat ($\alpha \sim 3$) pushers. The blue dashed line represents the theoretical threshold for capsules with low-adiabat ($\alpha \sim 1.5$) pushers. The open circles are the NIF data. By this criterion, N210808 achieved ignition in the hot spot [6].

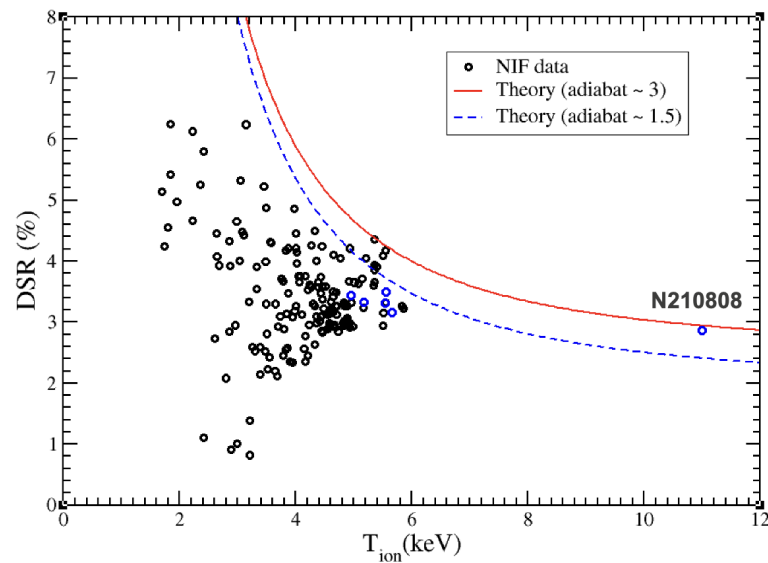


Figure 3. The minimum required DSR of the capsules for self-sustained TN burn as a function of the hot-spot temperature. The red solid line is the theoretical threshold for capsules with high-adiabat ($\alpha \sim 3$) pushers. The blue dashed line represents the theoretical threshold for capsules with low-adiabat ($\alpha \sim 1.5$) pushers. The open circles are the NIF data. The blue open circles are the shots listed in Table 2. N210808 achieved ignition in the hot spot.

The ignition threshold on DSR is expected to be less rigorous and also weaker than the ignition threshold on $\tilde{\nu}$. As demonstrated in Figures 2 and 3, at about 5.5 keV of the hot-spot temperature, several NIF shots that seemed very close to the ignition curve of DSR in Figure 3 are actually far below the ignition threshold of $\tilde{\nu}$ in Figure 2. The reason for such a discrepancy is that the threshold for $\tilde{\nu}$ is directly derived from the hot-spot $\rho R - T$ ignition condition, while the threshold on DSR is translated from the total areal density of the DT, which depends on model approximations for the relationship between the hot-spot areal density and the total areal density of the DT. The total areal density of the fuel plays less of a role in fusion performance of the capsules than the areal density of the hot spot. The critical difference between them has been discussed in article [33]. As such, the ignition threshold on DSR is more relaxed and less restricted than the $\rho R - T$ ignition condition that is directly equivalent to the Lawson criterion.

Figures 2 and 3 show that the thresholds on both $\tilde{\nu}$ and DSR for self-sustained TN burn decrease with the increase in (or runaway of) the hot-spot temperature. Experimental data show that NIF shots with high performance have observed specific energy ratios $\tilde{\nu}_0$ typically at values around 0.12–0.15. The reason that high-performance capsules have low measured $\tilde{\nu}$ is not because of a low energy conversion from the implosion energy to the internal energy, but due to the alpha energy deposition and heating that increase the hot-spot temperature.

A similar analysis applies to the DSR. In high-performance capsules, the TN burn in the hot spot is intense and may launch burn propagation. The burn propagation wave heats up the surrounding higher-density cold DT fuel and ablates them into lower-density hot fuel, which decreases the total fuel areal density of the DT (the sum of hot and cold fuel) in the capsules and, in turn, the DSR, as observed in a number of recent high-yields shot in the hybrid series given in Table 2 [1,38] (particularly, shot N210808 [6]).

Table 2. Experimental data from recent high-yield shots on NIF [1,6,38].

Shot	Y (kJ)	T_{hs} (keV)	DSR (%)	V_{imp} (km/s)	$(\rho R)_{hs}$ (g/cm ²)	\tilde{v}_0
N201101	98.4	4.95	3.44	383		0.123
N201122	106.2	5.17	3.33	376		0.114
N210207	170	5.66	3.16	389	0.37	0.111
N210220	160.6	5.54	3.31	369		0.102
N210307	145	5.55	3.49	385	0.38	0.112
N210808	1370	11	2.87	391	0.456	0.06

As an example, we consider an ignition capsule with pusher mass $M_p \simeq 340 \mu\text{g}$, high pusher adiabat ($\alpha \sim 3$, $\gamma_p \sim 5/3$), initial outer radius $R_0 \simeq 1000 \mu\text{m}$, convergence ratio $C_f \approx 30$, and peak no-burn hot-spot temperature $T \simeq 4.8 \text{ keV}$. Substituting these numbers into Equations (13) and (15) gives the thresholds of the peak no-burn $\tilde{v} \geq 0.37$ and the downscatter ratio $DSR \geq 0.055$ for the hot spot of the capsule to have self-sustained TN burn. All of the observed specific energy ratios in the NIF shots, plotted in Figure 2, are lower than the peak no-burn \tilde{v} , as expected.

3. Discussions

3.1. Important Time Scales

We performed an analysis of the recent NIF high-yield shot N210808 using the publicly announced data [1,6]. According to the NIF announcement [1,39], the capsule in N210808 has a measured neutron yield $\sim 4.3 \times 10^{17}$, hot-spot radius $R_{hs} \sim 51.2 \mu\text{m}$, and average hot-spot temperature $T_{hs} \sim 11 \text{ keV}$. The neutron downscatter ratio for this capsule is about $2.87\% \pm 0.1\%$ and the peak implosion velocity is approximately $391 \mu\text{m/ns}$. Using these numbers, we can estimate the average nuclear reproduction time in the capsule during the TN burn, $\tau_{rep} \simeq E/[N_D N_T \langle \sigma v \rangle W_\alpha / V] \sim 28 \text{ ps}$, which is significantly shorter than the hydrodynamic disassembly time, $\tau_H = R_{hs}/C_s \sim 42.8 \text{ ps}$, of the capsule that is required for achieving self-sustained TN burn. Here, $f_T \simeq 1$ was used to be conservative. Clearly, the TN burn in N210808 was self-sustained for a period of time.

It is worthwhile to point out that the nuclear energy reproduction time is an important time scale in fusion. It is different from burn width and confinement time. It is the time required for an equal amount of energy to be liberated by thermonuclear DT reactions or the time required for the energy of the hot fuel to *double itself (e-folding) and achieve self-sustained thermonuclear burn at or above the critical ignition temperature and areal density* as a result of DT interactions. This quantity measures the nuclear energy reproduction rate of the system. It is a useful concept for comparing the competing processes of heating versus cooling at various densities and temperatures per unit time in a system. The confinement time in nuclear fusion devices is defined as the time the plasma is maintained *at a temperature and an areal density above the critical ignition temperature and areal density and has self-sustained burn*, which is completely different from the burn time (or burn width) of the capsule. Burn time is defined as the full burn width at half maximum (FWHM) or the time period during which at least 50% of the maximum neutron production rate is observed [24–26]. Different definitions of burn width and confinement time can be found in [40]. Obviously, every NIF experiment has a full burn width, but not every experiment has a non-zero confinement time and self-sustained burn. For example, most of the early NIF shots, conducted during the National Ignition Campaign, had very long burn width, but no alpha-heating. The confinement time in those shots was nearly zero because the necessary condition $\tau_{rep} < \tau_H$ was never achieved and the DT hot spot was never burnt near the critical $\rho R - T$ ignition condition.

According to our analysis, the ignition capsule in N210808 had self-sustained TN burn for a short period of time during which $\tau_{rep} \leq \tau_H$ was satisfied and burn propagation was launched. However, the mass of the adjacent cold DT fuel swept up by the propagating sound wave was too large to be heated enough to burn. For example, the cold mass swept by the

burn wave within ~ 4 ps of propagation would be comparable to the hot-spot mass itself, so the TN burn front would be stopped, as indicated in the diagnostic data of the shot [6].

The existence of such a momentary burn propagation in the N210808 may have revealed some unexpected challenges to hot-spot ignition via burn propagation, which require an extensive and robust hot-spot burn front that seems hard to be produced reliably on the current NIF. The measured specific energy ratio in N210808 is $\tilde{v}_0 \approx 0.06$. The low value of \tilde{v}_0 and the observed ignition on the hot spot of N210808 suggest that the peak no-burn temperature of the hot spot in N210808 may be higher than the announced 4.9 keV, as indicated by post-shot simulations, and the peak implosion velocity may be higher than the released 391 km/s in order to be consistent with the measured neutron yield, hot-spot sizes and temperatures, and TN burn width in N210808.

Researchers may think that the observed hot-spot ignition in N210808 contradicts the required laser energy of 10 MJ to ignite a high-adiabat target given by the authors in reference [25]. Here, we would like to point out that the minimum required laser energy (E_L^{min}) or the minimal peak implosion kinetic energy (E_{pk}^{min}) for achieving ignition on NIF depend on the energy-coupling efficiency, $\eta\eta_L$, where η_L is the conversion efficiency of the laser energy to the peak pusher kinetic energy, $E_{pk}^{min} = \eta_L\eta E_L^{min}$. It has expression [24,25] $E_L^{min} \geq 2RT(3\gamma_p - 1)M_{hs} / [A_{DT}\eta_L\eta(\gamma_p - 1)(\gamma_g - 1)] \approx 0.1157 \times 10^{-4}(3\gamma_p - 1)(M_{hs}/\mu g)(T/\text{keV}) / [\eta_L\eta(\gamma_p - 1)]$ MJ [24]. For $\eta_L\eta \approx 1.6\%$, as in most NIF high-foot experiments, substituting the minimum required hot-spot mass of 40 μg for ignition at $T = 4$ keV and convergence ratio of 27 into the expression, we obtain $E_L^{min} \geq 10$ MJ or $E_{pk}^{min} \geq 160$ kJ for a high pusher adiabat ($\alpha \sim 3, \gamma_p \approx 3$) target. Recent improvements in the Hybrid-E design have increased the energy-coupling coefficients significantly, for example, in shot N210808, $\eta_L\eta \approx 6.7\%$ (about 4.2 times higher than the number of 1.6% used in Ref. [2,3,6,24,25]). Substituting this improved energy efficiency into the expression of the minimal laser energy, we obtain the required laser energy to ignite a high-adiabat target, $E_L^{min} \geq 10/4.2 \approx 2.39$ MJ, which is consistent with the ongoing NIF experimental data [1,2,6,41]. With continuing improvements of energy-coupling efficiency, high yield with lower required laser energy on NIF becomes possible.

The dependence of the neutron yield upon the measured specific energy ratio in the NIF experiments is plotted in Figure 4. In the figure, the recent high-yield shots listed in Table 2 are plotted in blue circles, which are shown to be very well behaved and uniquely lined-up in a straight line, which is also consistent with the trend line shown in previous ignition experiments.

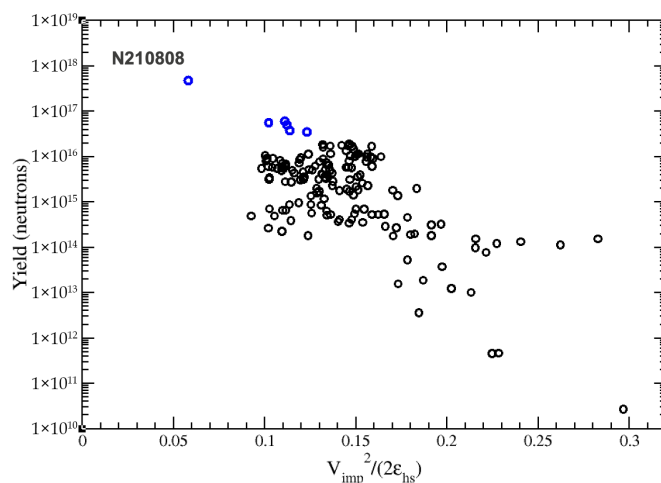


Figure 4. Neutron yield vs. observed specific energy ratio in the NIF shots.

3.2. Comparison of Ignition Metrics

Compared to other ignition metrics, for example, the metrics listed in Table 2 in reference [6], important differences among them are worth noting. The generalized Lawson criterion, $GLC_L > 1$, derived by Lindl et al. [42], is expressed in terms of time-averaged hot-spot pressure and radius and based upon a definition of ignition as a yield amplification of 30 (yield ratio of α -on to no- α), which corresponds to the doubling of the hot-spot temperature. The value of the threshold was calibrated to fit the large 1D simulations. This metric describes the resultant behavior of ignition but cannot tell when ignition would occur prior to ignition. An improved form, GLC_H , was derived by Hurricane et al. [32,43–45] from thermodynamics by defining ignition (or self-heating) as a point of breaking adiabaticity of the hot spot. This metric takes into account some 3D effects. The threshold was determined from power balance between α -heating and energy losses through radiation, thermal conduction, and mechanical work, particularly by requiring hot-spot pressure increase ($\partial P_{hs}/\partial V \geq 0$) after stagnation. $GLC_H = 1$ corresponds to a yield amplification of 16–32 according to simulations. However, the appearance of breaking adiabaticity of hot spot and hot-spot pressure increase after stagnation do not necessarily ensure an ignition or self-sustained TN burn in the hot spot. The reasons are (i) the hot-spot itself in the NIF point design is an open system; it continuously gains mass from the ablation of the cold DT fuel during implosion and explosion, so the compression process is not adiabatic and the product PV^γ is not conserved for the hot spot during the entire process; and (ii) in addition to the identified energy losses (radiation, thermal conduction and mechanical work), there are other unlisted energy losses, for example, non-radial kinetic energy of the shell (e.g., rotational, vibrational, etc.). Thus, $\partial P_{hs}/\partial V \geq 0$ may not guarantee that the hot-spot temperature will not drop below the ignition temperature momentarily due to other energy losses. Therefore, the criterion given by this condition is relatively weaker than the criterion $GLC_L > 1$. Similar to metric GLC_L , the ignition condition, $E_\alpha/E_{hs} > 1.4$, proposed by Christopherson et al. [46] was obtained by fitting the 1D simulations from LILAC and 2D simulations from DRACO [46]. This threshold corresponds to a yield amplification of 20–30. Similar arguments apply to the ignition threshold experiment metric (ITFX) and its most up-to-date version [6,15]. ITFX is a complicated function of the metric with α -on ($ITFX_\alpha$), calibrated to large simulations in terms of fuel mass and DSR. A common feature of these ignition thresholds is that they depend on the calibrated simulations and vary with simulations. Considering the fact that simulations are generally optimistic, the simulation fitted criteria are, thus, usually weaker than the requirements in real experiments.

Several analytical ignition metrics and thresholds have been proposed by researchers. Similar to the metric GLC_H , the ignition condition given by Atzeni et al. [47] was derived from power balance by taking into account the power losses from bremsstrahlung radiation, thermal conduction, and mechanic work (ignored for isobaric model) and expressed in terms of a $\rho R - T$ condition. Because of the neglect of other energy losses, this metric has the same weakness as metric GLC_H and gives a lower threshold than the other ignition metrics. The ignition condition presented by Cheng et al. is different from all above metrics. In this model, the ignition criterion is derived by requiring the nuclear energy reproduction time (i.e., the hot-spot energy doubling time) in the hot DT fuel being less than the hydrodynamic disassembly time (R_{hs}/C_s) during TN burn, which leads to a $\rho R - T$ condition [23–25,33]. The energy doubling requirement in this framework ensures the self-sustained TN burn maintained at or above the ignition temperature and areal density in the hot fuel and all of the energy losses (both identified and unidentified) that decrease the temperature of the hot fuel compensated. The fusion confinement time is the duration of the TN burn at or above the ignition temperature and areal density. Thus, the ignition criterion given by this model is more pessimistic than the other metrics. Here, we would like to point out that the ignition condition by Tipton [48] is similar to the condition by Cheng et al.—the only difference is in the approximation of the DT reaction rate $\langle \sigma v \rangle_{DT}$. The ignition criterion by Coutant [49] was obtained by using 1/4 of hydrodynamic disassembly time for fusion confinement time in the Lawson criterion. Thus, the Coutant condition seems more

stringent than all other thresholds. Using $1/4$ instead of one hydrodynamic disassembly time is a good idea to account for any 3D effects, hydrodynamic instabilities, and turbulence in the capsules [50–53]. In our view, condition $d^2T/dt^2 > 0$ [43] has minimal information because the condition itself does not specify whether the hot spot is at or above ignition temperature and whether the TN burn in the hot spot is self-sustained. The threshold only means that the hot-spot temperature is increasing with time and ensures that the condition at $dT/dt = 0$ [43] is a minimum, not a maximum.

Because threshold Equation (13) for \tilde{v} is directly derived from the $\rho R - T$ condition by Cheng et al. [23–25,33], compared with other metrics, metric \tilde{v} shows a number of advantages. First, metric \tilde{v} has a definite and clear physical meaning, i.e., it represents the ratio of the specific kinetic energy of implosion to the internal energy of the hot spot at peak compression. \tilde{v} characterizes how the kinetic energy of implosion was converted into internal energy of the capsule during implosion and, in turn, reflects the quality of implosion of the capsule. Second, metric \tilde{v} is analytic and independent of code simulations and models. And third, metric \tilde{v} is observable from experiments. We point out that, although the peak implosion velocity cannot be directly measured with the current diagnostic technology in the same experiment in which the temperature is determined, it can be measured in a separate convergent ablator, or “Con A,” experiment [54] by keeping the same implosion conditions as in previous experiments. In this sense, ratio \tilde{v} can be viewed as a measured metric.

4. Conclusions

The new physical metric \tilde{v} —the ratio of the specific peak implosion energy to the specific internal energy of the hot spot—captures the improvements in performance during the design process of fusion capsules. Additionally, it quantifies the energy conversion of the capsule from the implosion kinetic energy of the pusher shell into the internal energy of the hot fuel and the degree of alpha heating, as well as the possible burn propagation in the capsules. Our results show that the specific energy ratio of the hot spot and the DSR of the capsules decrease with increasing hot-spot temperature, alpha heating, and the launching of burn propagation from the hot spot into the cold fuel (as does the ignition threshold). These results are consistent with recent NIF experiments. This new metric can provide a new perspective to the NIF experiments by which the performance of the burning plasma can be determined and controlled through the fine-tuning of the implosion parameters, which helps future point designs and can be applied to the double-shell designs as well.

Author Contributions: Conceptualization, B.C. and P.A.B.; Methodology, B.C. and P.A.B.; Validation, B.C. and P.A.B.; Data collection, B.C. and P.A.B.; Analysis, B.C. and P.A.B.; Writing, B.C. and P.A.B. All authors have contributed equally in the developments of theory, methodology, validation and formal analysis. All authors read and agreed to the published version of the manuscript.

Funding: This research received no external funding.

Data Availability Statement: Data sharing is not applicable.

Acknowledgments: The authors are grateful to O. L. Landen for his detailed NIF data summary and valuable analysis. This work was supported by the LANL ICF program and performed under the auspices of the U.S. Department of Energy by the Los Alamos National Laboratory under Contract No. 89233218CNA000001.

Conflicts of Interest: The authors declare no conflict of interest.

References

1. Kritcher, A.L.; Zylstra, A.B.; Callahan, D.A.; Hurricane, O.A.; Weber, C.R.; Clark, D.S.; Young, C.V.; Ralph, J.E.; Casey, D.T.; Pak, A.; et al. Design of an inertial fusion experiment exceeding the Lawson criterion for ignition. *Phys. Rev. E* **2022**, *106*, 025201. [[CrossRef](#)]
2. Kritcher, A.L.; Young, C.V.; Robey, H.F.; Weber, C.R.; Zylstra, A.B.; Hurricane, O.A.; Callahan, D.A.; Ralph, J.E.; Ross, J.S.; Baker, K.L.; et al. Design of inertial fusion implosions reaching the burning plasma regime. *Nat. Phys.* **2022**, *18*, 251–258. [[CrossRef](#)]

3. Zylstra, A.B.; Kritcher, A.L.; Hurricane, O.A.; Callahan, D.A.; Ralph, J.E.; Casey, D.T.; Pak, A.; Landen, O.L.; Bachmann, B.; Baker, K.L.; et al. Experimental achievement and signatures of ignition at the National Ignition Facility. *Phys. Rev. E* **2022**, *106*, 025202. [[CrossRef](#)]
4. Kritcher, A.L.; Zylstra, A.B.; Callahan, D.A.; Hurricane, O.A.; Weber, C.; Ralph, J.; Casey, D.T.; Pak, A.; Baker, K.; Bachmann, B.; et al. Achieving record hot spot energies with large HDC implosions on NIF in HYBRID-E. *Phys. Plasmas* **2021**, *28*, 072706. [[CrossRef](#)]
5. Zylstra, A.B.; Kritcher, A.L.; Hurricane, O.A.; Callahan, D.A.; Baker, K.; Braun, T.; Casey, D.T.; Clark, D.; Clark, K.; Döppner, T.; et al. Record Energetics for an Inertial Fusion Implosion at NIF. *Phys. Rev. Lett.* **2021**, *126*, 025001. [[CrossRef](#)]
6. Abu-Shawared, H.; Acree, R.; Adams, P.; Adams, J.; Addis, B.; Aden, R.; Adrian, P.; Afeyan, B.B.; Aggleton, M.; Aghaian, L.; et al. (Indirect Drive ICF Collaboration), Lawson's criteria for ignition exceeded in an inertial fusion experiment. *Phys. Rev. Lett.* **2022**, *129*, 075001. [[CrossRef](#)]
7. Abu-Shawared, H.; Acree, R.; Adams, P.; Adams, J.; Addis, B.; Aden, R.; Adrian, P.; Afeyan, B.B.; Aggleton, M.; Aghaian, L.; et al. (Indirect Drive ICF Collaboration), Achievement of Target Gain Larger than Unity in an Inertial Fusion Experiment. *Phys. Rev. Lett.* **2024**, *132*, 065102. [[CrossRef](#)]
8. Thomas, C.A.; Campbell, E.M.; Baker, K.L.; Casey, D.T.; Hohenberger, M.; Kritcher, A.L.; Spears, B.K.; Khan, S.F.; Nora, R.; Woods, D.T.; et al. Principal factors in performance of indirect-drive laser fusion experiments. *Phys. Plasmas* **2020**, *27*, 112712. [[CrossRef](#)]
9. Hopkins, L.F.B.; Pape, S.L.; Pak, L.D.N.A.; Dewald, E.L.; Ho, D.D.; Bhandarkar, N.; Bhandarkar, S.; Benedetti, L.R.; Bunn, T.; Biener, J.; et al. Toward a burning plasmas state using diamond ablator inertially coned 11 fusion (ICF) implosions on the National Ignition Facility. *Plasma Phys. Control. Fusion* **2019**, *61*, 014023. [[CrossRef](#)]
10. Pape, S.L.; Hopkins, L.F.B.; Divol, L.; Pak, A.; Dewald, E.L.; Bhandarkar, S.; Benedetti, L.R.; Bunn, T.; Biener, J.; Crippen, J.; et al. Fusion energy output greater than the kinetic energy of an imploding shell at the National Ignition Facility. *Phys. Rev. Lett.* **2018**, *120*, 245003. [[CrossRef](#)]
11. Thomas, C.A.; Campbell, E.M.; Baker, K.L.; Casey, D.T.; Hohenberger, M.; Kritcher, A.L.; Spears, B.K.; Khan, S.F.; Nora, R.; Woods, D.T.; et al. Experiments to explore the influence of pulse shaping at the National Ignition Facility. *Phys. Plasmas* **2020**, *27*, 112708. [[CrossRef](#)]
12. Dewald, E.L.; Tommasini, R.; Meezan, N.B.; Landen, O.L.; Khan, S.; Rygg, R.; Field, J.; Moore, A.S.; Sayre, D.; MacKinnon, A.J.; et al. First demonstration of improved capsule implosions by reducing radiation preheat in uranium versus gold hohlraums. *Phys. Plasmas* **2018**, *25*, 092702. [[CrossRef](#)]
13. Casey, D.T.; Thomas, C.A.; Baker, K.L.; Spears, B.; Hohenberger, M.; Khan, S.F.; Nora, R.C.; Weber, C.R.; Woods, D.T.; Hurricane, O.; et al. The high velocity, high adiabat, bigfoot campaign and test of indirect-drive implosion scaling. *Phys. Plasmas* **2018**, *25*, 056308. [[CrossRef](#)]
14. Baker, K.L.; Thomas, C.A.; Casey, D.; Khan, S.; Spears, B.K.; Nora, R.; Woods, T.; Milovich, J.; Berger, R.L.; Strozzi, D.; et al. High-performance indirect-drive cryogenic implosions at high adiabat on the National Ignition Facility. *Phys. Rev. Lett.* **2018**, *121*, 135001. [[CrossRef](#)] [[PubMed](#)]
15. Patel, P.K.; Springer, P.T.; Weber, C.R.; Jarrott, L.C.; Hurricane, O.A.; Bachmann, B.; Baker, K.L.; Hopkins, L.F.B.; Callahan, D.A.; Casey, D.T.; et al. Hotspot conditions achieved in inertial confinement fusion experiments on the National Ignition Facility. *Phys. Plasmas* **2020**, *27*, 050901. [[CrossRef](#)]
16. Landen, O.L.; Casey, D.T.; Nicola, J.M.D.; Doeppner, T.; Hartouni, E.P.; Hinkel, D.E.; Hopkins, L.F.B.; Hohenberger, M.; Kritcher, A.L.; Pape, S.L.; et al. Yield and compression trends and reproducibility at NIF. *High Energy Density Phys.* **2020**, *36*, 100755. [[CrossRef](#)]
17. Clark, D.S.; Kritcher, A.L.; Yi, S.A.; Zylstra, A.B.; Haan, S.W.; Weber, C.R. Capsule physics comparison of National Ignition Facility implosion designs using plastic, high density carbon, and beryllium ablaters. *Phys. Plasmas* **2018**, *25*, 032703. [[CrossRef](#)]
18. Clark, D.S.; Weber, C.R.; Milovich, J.L.; Pak, A.E.; Casey, D.T.; Hammel, B.A.; Ho, D.D.; Jones, O.S.; Koning, J.M.; Kritcher, A.L.; et al. Three-dimensional modeling and hydrodynamic scaling of National Ignition Facility implosions. *Phys. Plasmas* **2019**, *26*, 050601. [[CrossRef](#)]
19. Thomas, C.A.; Campbell, E.M.; Baker, K.L.; Casey, D.T.; Hohenberger, M.; Kritcher, A.L.; Spears, B.K.; Khan, S.F.; Nora, R.; Woods, D.T.; et al. Deficiencies in compression and yield in x-ray driven implosions. *Phys. Plasmas* **2020**, *27*, 112705. [[CrossRef](#)]
20. Gaffney, J.A.; Brandon, S.T.; Humbird, K.D.; Kruse, M.K.G.; Nora, R.C.; Peterson, J.L.; Spears, B.K. Making inertial confinement fusion models more predictive. *Phys. Plasmas* **2019**, *26*, 082704. [[CrossRef](#)]
21. Pak, A.; Divol, L.; Weber, C.R.; Hopkins, L.F.B.; Clark, D.S.; Dewald, E.L.; Fittinghoff, D.N.; Geppert-Kleinrath, V.; Hohenberger, M.; Pape, S.L.; et al. Impact of Localized Radiative Loss on Inertial Confinement Fusion Implosions. *Phys. Rev. Lett.* **2020**, *124*, 145001. [[CrossRef](#)]
22. Park, H.-S.; Hurricane, O.A.; Callahan, D.A.; Casey, D.T.; Dewald, E.L.; Dittrich, T.R.; Döppner, T.; Hinkel, D.E.; Hopkins, L.F.B.; Pape, S.L.; et al. High-Adiabat High-Foot Inertial Confinement Fusion Experiments on the National Ignition Facility. *Phys. Rev. Lett.* **2014**, *112*, 055001. [[CrossRef](#)]
23. Cheng, B.; Kwan, T.J.T.; Wang, Y.-M.; Batha, S.H. Scaling laws for ignition at the National Ignition Facility from first principles. *Phys. Rev. E* **2013**, *88*, 041101. [[CrossRef](#)]
24. Cheng, B.; Kwan, T.J.T.; Wang, Y.M.; Yi, S.A.; Batha, S.H.; Wysocki, F.J. Ignition and pusher adiabat. *Phys. Control. Fusion* **2018**, *60*, 074011. [[CrossRef](#)]

25. Cheng, B.; Bradley, P.A.; Finnagan, S.A.; Thomas, C.A. Fundamental factors affecting thermonuclear ignition. *Nucl. Fusion* **2020**, *61*, 096010. [[CrossRef](#)]
26. Cheng, B.; Kwan, T.J.T.; Wang, Y.M.; Merrill, F.E.; Cerjan, C.J.; Batha, S.H. Analysis of NIF experiments with the minimal energy implosion model. *Phys. Plasmas* **2015**, *22*, 082704. [[CrossRef](#)]
27. Cheng, B.; Kwan, T.J.T.; Wang, Y.M.; Yi, S.A.; Batha, S.H.; Wysocki, F.J. Effects of preheat and mix on the fuel adiabat of an imploding capsule. *Phys. Plasmas* **2016**, *23*, 120702. [[CrossRef](#)]
28. Melvin, J.; Lim, H.; Rana, V.; Cheng, B.; Glimm, J.; Sharp, D.H.; Wilson, D.C. Sensitivity of inertial confinement fusion hot spot properties to the deuterium-tritium fuel adiabat. *Phys. Plasmas* **2015**, *22*, 022708. [[CrossRef](#)]
29. Hurricane, O.A.; Callahan, D.A.; Casey, D.T.; Dewald, E.L.; Dittrich, T.R.; Döppner, T.; Haan, S.; Hinkel, D.E.; Hopkins, L.F.B.; Jones, O.; et al. Inertially confined fusion plasmas dominated by alpha-particle self-heating. *Nat. Phys.* **2016**, *12*, 800–806. [[CrossRef](#)]
30. Callahan, D.A.; Hurricane, O.A.; Hinkel, D.E.; Döppner, T.; Ma, T.; Park, H.-S.; Garcia, M.A.B.; Hopkins, L.F.B.; Casey, D.T.; Cerjan, C.J.; et al. Higher velocity, high-foot implosions on the National Ignition Facility laser. *Phys. Plasmas* **2015**, *22*, 056314. [[CrossRef](#)]
31. Haan, S.W.; Lindl, J.D.; Callahan, D.A.; Clark, D.S.; Salmonson, J.D.; Hammel, B.A.; Atherton, L.J.; Cook, R.C.; Edwards, M.J.; Glenzer, S.; et al. Point design targets, specifications, and requirements for the 2010 ignition campaign on the National Ignition Facility. *Phys. Plasmas* **2011**, *18*, 051001. [[CrossRef](#)]
32. Hurricane, O.A.; Springer, P.T.; Patel, P.K.; Callahan, D.A.; Baker, K.; Casey, D.T.; Divol, L.; Döppner, T.; Hinkel, D.E.; Hohenberger, M.; et al. Approaching a burning plasma on the NIF. *Phys. Plasmas* **2019**, *26*, 052704. [[CrossRef](#)]
33. Cheng, B.; Kwan, T.J.T.; Wang, Y.-M.; Batha, S.H. 'On Thermonuclear ignition criterion at the National Ignition Facility. *Phys. Plasmas* **2014**, *21*, 102707. [[CrossRef](#)]
34. Ballabio, L.; Källne, J.; Gorini, G. Relativistic calculation of fusion product spectra for thermonuclear plasmas. *Nucl. Fusion* **1998**, *38*, 1723. [[CrossRef](#)]
35. Murphy, T.J. The effect of turbulent kinetic energy on inferred ion temperature from neutron spectra. *Phys. Plasmas* **2014**, *21*, 072701. [[CrossRef](#)]
36. Krokhin, O.N.; Rozanov, V.B. Escape of α particles from a laser-pulse-initiated thermonuclear reaction. *Sov. J. Quantum Electron.* **1973**, *2*, 393. [[CrossRef](#)]
37. Cheng, B.; Kwan, T.J.T.; Yi, S.A.; Landen, O.L.; Wang, Y.M.; Cerjan, C.J.; Batha, S.H.; Wysocki, F.J. Effects of asymmetry and hot-spot shape on ignition capsules. *Phys. Rev. E* **2018**, *98*, 023203. [[CrossRef](#)]
38. Zylstra, A.B.; Hurricane, O.A.; Callahan, D.A.; Kritcher, A.L.; Ralph, J.E.; Robey, H.F.; Ross, J.S.; Young, C.V.; Baker, K.L.; Casey, D.T.; et al. 2022 Burning plasma achieved in inertial fusion. *Nature* **2022**, *601*, 542–548. [[CrossRef](#)]
39. Herrmann, M. *Recent Inertial Confinement Fusion Results from the National Ignition Facility*; NIF Press: Livermore, CA, USA, 2021.
40. Hurricane, O.A.; Maclaren, S.A.; Rosen, M.D.; Hammer, J.H.; Springer, P.T.; Betti, R. A thermodynamic condition for ignition and burn-propagation in cryogenic layer inertially confined fusion implosions. *Phys. Plasmas* **2021**, *28*, 022704. [[CrossRef](#)]
41. Kritcher, A.L.; Zylstra, A.B.; Weber, C.R.; Hurricane, O.A.; Callahan, D.A.; Clark, D.S.; Divol, L.; Hinkel, D.E.; Humbird, K.; Jones, O.; et al. Design of the first fusion experiment to achieve target energy gain $G > 1$. *Phys. Rev. E* **2024**, *109*, 025204. [[CrossRef](#)]
42. Lindl, J.D. Haan, S.W., Christopherson, A.R., Betti, R. Progress toward a self-consistent set of 1D ignition metrics in ICF. *Phys. Plasmas* **2018**, *25*, 122704. [[CrossRef](#)]
43. Springer, P.T.; Hurricane, O.A.; Hammer, J.H.; Betti, R.; Callahan, D.A.; Campbell, E.M.; Casey, D.T.; Cerjan, C.J.; Cao, D.; Dewald, E.; et al. A 3D dynamic model to assess the impacts of low-mode asymmetry, aneurysms and mix-induced radiative loss on capsule performance across inertial confinement fusion platforms. *Nucl. Fusion* **2019**, *59*, 032009. [[CrossRef](#)]
44. Hurricane, O.A.; Casey, D.T.; Landen, O.; Kritcher, A.L.; Nora, R.; Patel, P.K.; Gaffney, J.A.; Humbird, K.D.; Field, J.E.; Kruse, M.K.G.; et al. An analytic asymmetric-piston model for the impact of mode-1 shell asymmetry on ICF implosions. *Phys. Plasmas* **2020**, *27*, 062704. [[CrossRef](#)]
45. Hurricane, O.A.; Callahan, D.A.; Springer, P.T.; Edwards, M.J.; Patel, P.; Baker, K.; Casey, D.T.; Divol, L.; Döppner, T.; Hinkel, D.E.; et al. Beyond alpha-heating: Driving inertially confined fusion implosions toward a burning-plasma state on the National Ignition Facility. *Plasma Phys. Control. Fusion* **2018**, *61*, 014033. [[CrossRef](#)]
46. Christopherson, A.R.; Betti, R.; Miller, S.; Gopalaswamy, V.; Mannon, O.M.; Cao, D. Theory of ignition and burn propagation in inertial fusion implosions. *Phys. Plasmas* **2020**, *27*, 052708. [[CrossRef](#)]
47. Atzeni, S.; Meyer-Ter-Vehn, J. *The Physics of Inertial Fusion*; Clarendon Pres: Oxford, UK, 2004.
48. Tipton, R. *Generalized Lawson Criteria for Inertial Confinement Fusion*; LLNL Report No. LLNL-TR-67692 (2015), Private Communications and Preprint; Lawrence Livermore National Lab.: Livermore, CA, USA, 2015.
49. Coutant, J. *La Fusion Thermonucleaire Inertielle Par Laser*; Dautray, R., Watteau, J.-P., Eds.; Eyrolles: Paris, France, 1993.
50. Zhou, Y.; Williams, R.J.; Ramaprabhu, P.; Groom, M.; Thornber, B.; Hillier, A.; Mostert, W.; Rollin, B.; Balachandar, S.; Powell, P.D.; et al. Rayleigh–Taylor and Richtmyer–Meshkov instabilities: A journey through scales. *Phys. D* **2021**, *423*, 132838. [[CrossRef](#)]
51. Zhou, Y.; Clark, T.T.; Clark, D.S.; Gail, Glendinning, S.; Skinner, M.A.; Huntington, C.M.; Hurricane, O.A.; Dimits, A.M.; Remington, B.A. Turbulent mixing and transition criteria of flows induced by hydrodynamic instabilities. *Phys. Plasmas* **2019**, *26*, 080901. [[CrossRef](#)]
52. Zhou, Y. Rayleigh–Taylor and Richtmyer–Meshkov instability induced flow, turbulence, and mixing. I. *Phys. Rep.* **2017**, *720–722*, 1–136. [[CrossRef](#)]

-
53. Zhou, Y. Rayleigh-Taylor and Richtmyer-Meshkov instability induced flow, turbulence, and mixing. II. *Phys. Rep.* **2017**, *723–725*, 1–116. [[CrossRef](#)]
 54. Hicks, D.G.; Meezan, N.B.; Dewald, E.L.; Mackinnon, A.J.; Olson, R.E.; Callahan, D.A.; Döppner, T.; Benedetti, L.R.; Bradley, D.K.; Celliers, P.M.; et al. Implosion dynamics measurements at the National Ignition Facility. *Phys. Plasmas* **2012**, *19*, 122702. [[CrossRef](#)]

Disclaimer/Publisher’s Note: The statements, opinions and data contained in all publications are solely those of the individual author(s) and contributor(s) and not of MDPI and/or the editor(s). MDPI and/or the editor(s) disclaim responsibility for any injury to people or property resulting from any ideas, methods, instructions or products referred to in the content.